

# Self-consistent 3D fluid modelling of the interaction between flushed and reciprocating probes and a turbulent Scrape-Off-Layer

R. Futersack<sup>1\*</sup>, P. Tamain<sup>1</sup>, G. Ciraolo<sup>1</sup>, C. Colin<sup>2</sup>, N. Fedorczak<sup>1</sup>, Ph. Ghendrih<sup>1</sup>, Y. Marandet<sup>3</sup>, F. Schwander<sup>2</sup>, et E. Serre<sup>2</sup>

<sup>1</sup> CEA-IRFM, F-13108 Saint-Paul-lez-Durance, France

<sup>2</sup> Aix-Marseille Université, CNRS, Centrale Marseille, M2P2 UMR 7340, 13451 Marseille, France

<sup>3</sup> Aix-Marseille Université, CNRS, PIIM, UMR 7345, Marseille F-13397, France

Received XXXX, revised XXXX, accepted XXXX

Published online XXXX

**Key words** Langmuir, probes, plasma, turbulence, SOL, 3D

3D interplay between Langmuir probes (LP) and Scrape-Off-Layer (SOL) plasma turbulence is numerically investigated with the TOKAM3X fluid code. A flushed LP is modelled by biasing a part of the target plates surface. The probe is found to drive a polarization of the plasma and consequently to impact the transverse transport. The perturbation extends along the connected flux tube, and, depending on both the length of the field lines and the plasma collisionality, can reach the next solid obstacle and draw current from it. The characteristics of the SOL turbulent plasma in the shadow of a probe body are also heavily impacted. In consequence, synthetic Mach measurements differ significantly from one can expect of the classical Hutchinson theory.

Copyright line will be provided by the publisher

## 1 Introduction

Scrape-Off-Layer turbulence studies mostly rely on plasma fluctuations measurements by the means of Langmuir probes (LP) [1–8]. Despite their apparent simplicity, probes come with an historical and rather complex theory: first measurements of IV characteristics were initiated in 1923 by Langmuir [1] and after few years, he provided the bases of the *quasineutral* plasma-sheath theory [2, 3]. Some decades later, Bohm describes the effect of magnetic field on electrical probes and suggests his famous Bohm criterion [4] a large body of literature: describing ion collection physics [9–14], kinetic effects [15, 16] of electrons and perturbations due to polarization [17–21].

As the subject of LP measurements theory and induced perturbations of the plasma is substantial and complex, this paper aims only at looking the perturbations caused by the probe on transport properties. Previous studies, modelling this probe-plasma interaction by biasing the target plates in the 2D interchange code TOKAM2D, showed that the presence of a LP in ion saturation mode significantly disturbs the plasma. In fact, as in biasing experiments [22], the polarization of the flux tube connected to the LP leads to the formation of a convective cell, which acts then as a transport barrier preventing the turbulent plasma to reach the probe tip. Here, we look at the effect of the parallel dynamics on the perturbation, and we study for the first time the impact on the turbulent plasma of the immersion of an object into the SOL.

Whilst the ion collection theory has been built up over a long history, current transport induced by a biased probe has been largely forsaken. Yet, some experimental evidences published by Matthews, Pitts and Stangeby [11, 17] show that when a probe is polarized negatively with respect to the wall of the device,

This paper is organized as follows. In section 2 we present the TOKAM3X code [23] and the modelling of the synthetic probes in a 3D-slab geometry. In section 3, we analyse the plasma perturbations caused by the biasing of a LP flushed in the divertor. In section 4, we look at the case of a mobile probe, unbiased, plunged into the SOL, and use our synthetic data to reproduce Mach measurements. Section 5

---

\* Corresponding author E-mail: romain.futersack@gmail.com, Phone: +33 630 718 763

## 2 Synthetic probe modelling in the TOKAM3X fluid code

The TOKAM3X code has been developed in the framework of a long-term program dedicated to edge transport modelling. TOKAM3X solves the drift-reduced Braginskii conservative equations in an arbitrary 3D magnetic geometry (from limited to multiple X-points). The model is able to describe the core and the SOL plasmas, without any scale separation between the size of the device and those of plasma fluctuations allowing the code to recover, in a self-consistent way, large scale flows as well as the characteristic SOL electrostatic turbulence.

### 2.1 Fluid model of the SOL turbulent transport

The SOL plasma consists of electrons following a Boltzmann distribution and a single ion specie of mass  $m_i$  and charge  $e$ . The plasma is assumed quasineutral which allows to solve the current conservation  $\nabla \cdot \mathbf{j} = 0$  equation (in conjunction with the parallel Ohm's law) to recover the electrostatic potential. Perpendicular transport is described in term of drifts (electric, diamagnetic and polarization) assuming its characteristic frequency scale is small with respect to the ion gyro-frequency  $\omega_c = eB/m_i$ . Reference plasma density  $n_0$  and temperature  $T_0$  are then used to make dimensionless the fluid quantities and equations. The electrostatic potential  $\Phi$  is normalized to  $T_0/e$ , velocities to a thermal speed  $c_s = \sqrt{eT_0/m_i}$ , times to  $\omega_c^{-1}$  and lengths to  $\rho_L = c_s \omega_c^{-1}$  accordingly. Temperature distribution of electrons  $T_e$  and ions  $T_i$  are chosen uniform and equal, eg.  $T_e = T_i = 1$ .

In this work, equations are solved in a simplified 3D slab geometry, with  $X \equiv (r-a)/\rho_L$  and  $Y \equiv r\theta/\rho_L$ , both perpendicular to the magnetic field  $\mathbf{B} = B_0 \mathbf{b}$  ( $r$  and  $\theta$  being the minor radius and the poloidal angle coordinates and  $a$  the minor radius at the separatrix). The parallel direction is indicated by  $Z \equiv \varphi/\rho_L$ . All curvature terms are dropped except the divergence of the diamagnetic current which drives the interchange instability [18].

Conservation equations of the model then read:

$$\partial_t N + \nabla \cdot (N \mathbf{u}_E) - D \nabla_{\perp}^2 N = S - \nabla \cdot (N(\Gamma_{\parallel} - J_{\parallel}) \mathbf{b}/N) \quad (1)$$

$$\partial_t \Gamma_{\parallel} + \nabla \cdot (\Gamma_{\parallel} \mathbf{u}_E) - D_{\Gamma} \nabla_{\perp}^2 \Gamma_{\parallel} = -2 \nabla_{\parallel} N - \nabla \cdot (\Gamma_{\parallel}^2 \mathbf{b}/N) \quad (2)$$

$$J_{\parallel} = -\eta_{\parallel}^{-1} \nabla_{\parallel} (\Phi - \ln N) \quad (3)$$

$$\partial_t W + \nabla \cdot (W \mathbf{u}_E) - \nu \nabla_{\perp}^2 W = -g \nabla_y N + \nabla \cdot (J_{\parallel} \mathbf{b}) - \nabla \cdot (W \Gamma_{\parallel} \mathbf{b}/N) \quad (4)$$

The two first equations (1) and (2) correspond respectively to the conservation of electron density  $N$  and parallel ion momentum  $\Gamma_{\parallel}$ . Electron transport along magnetic field lines, neglecting inertia, leads to a parallel Ohm's law Eq. (3) relating the parallel current  $J_{\parallel}$  to the parallel gradients of the potential and pressure. Eq. (4) derives from the charge balance equation and involves the electric vorticity  $W = \nabla_{\perp}^2 \Phi$ , defined under a Boussinesq-like approximation. Together, Eqs. (3) and (4) give the electrostatic potential  $\Phi$ , and hence the electric field  $\mathbf{E} = -\nabla \Phi$ .

The electric drift velocity  $\mathbf{u}_E = \mathbf{E} \times \mathbf{B}/B^2$  advects mater, current and ion momentum across the magnetic field.  $\eta_{\parallel}$  is the parallel resistivity of the plasma while  $D$ ,  $\nu$  and  $D_{\Gamma}$  are diffusion coefficients, accounting for collisionnal processes. In Eq. (4), the divergence of the diamagnetic current is reduced to a curvature term proportionnal to  $g$ . Finally the system is flux-driven, with a density source term  $S$  (gaussian shape of radial length  $L_s$  and centered on  $X_s$ ) mimicking an incoming flux from the core.

We only consider the SOL, all magnetic field lines ends at the divertor plates, where Bohm boundary conditions are applied on particle fluxes and currents:

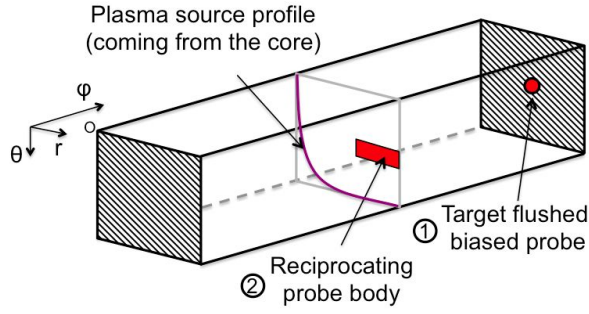
$$\Gamma_{\parallel se} = \pm N_{se} \exp(\Lambda - \Phi_{se}) \quad J_{\parallel se} = \pm N_{se} (1 - \exp(\Lambda - \Phi_{se}))$$

The *se* subscript is referring to the value of the quantity at the sheath entrance while  $\Lambda = \ln(m_i/2\pi m_e)/2$ , the normalized sheath potential drop, corresponds to the equilibrium potential which cancels out the sheath current and screens the wall from the plasma. In this paper, simulations are run on a 128x256x32 mesh, for a duration of typically  $10^5$  time steps with standard parameters of Table 1:

For a typical hydrogen discharge, with a magnetic field of  $B_0 = 3\text{T}$ , density around  $10^{19} \text{m}^{-3}$  and an electronic temperature equals to 100 eV, the Larmor radius  $\rho_L = 0.3 \text{mm}$  and the simulated plasma takes place in a narrow box of 87mm x 87mm x 8m. *The rather high collisionnality  $\eta_{\parallel}$  = and the length of field lines are then comparable to those of a small tokamak*

**Table 1** Standard values of non-dimentional control parameters used in the 3D simulations.

$dt$	$L_{  }$	$L_X$	$L_Y$	$\eta$	$\Lambda$	$g$	$D, D_{\Gamma} \text{ \& } \nu$	$S_0$	$X_s$	$L_s$
1	$12 \cdot 10^3$	256	256	$10^{-5}$	2.8388	$3 \cdot 10^{-3}$	$10^{-2}$	$10^{-2}$	32	8

**Fig. 1** Sketch of the slab geometry for the SOL. Divertor plates are located at the end of the field lines, depicted with hatchings. The flushed probe is situated in the center of the top divertor plate and the mobile probe inserted in the middle of the domain. The profile of the source term driving the system is aslo roughly indicated for comprehension purposes.

## 2.2 Synthetic probes models

The layout of the problem is illustrated in Fig. 1. In a first part, a biased probe is inserted in the center of the top divertor plate at  $Z_p = L_{||}$ . For the second part, the body of a swept probe is plunged into the SOL plasma, either at one-half of one-fourth of the field lines, ie.  $Z_p = L_{||}/2$  or  $Z_p = L_{||}/4$ .

The interaction between the probe and the SOL plasma is described by the sheath theory in strong magnetic fields, with field lines perpendicular to the wall [4]. The flushed probe is then modeled by a local polarization of the target plates, via a modification of the parallel Bohm boundary conditions :

$$\Gamma_{||p} = \pm N_p \exp(\Lambda - \Phi_p + \Phi_{wall}) \quad J_{||p} = \pm N_p (1 - \exp(\Lambda - \Phi_p + \Phi_{wall}))$$

$\Gamma_{||p}$ ,  $N_p$ ,  $\Phi_p$  and  $J_{||p}$  are plasma quantities in front of the probe but still at the sheath entrance. The wall polarization has a gaussian shape  $\Phi_{wall} = V_p \exp(-(X - X_p)^2/L_p^2) \exp(-(Y - Y_p)^2/L_p^2)$  with  $V_p$  the applied bias voltage,  $(X_p, Y_p)$  the position and  $L_p$  the size of the probe. In the limit of strong negative polarization<sup>1</sup>, the Boltzmann exponential term tend toward zero locally: only ions reach the probe and the current drawn by the probe is equal to the ion flux, ie. the probe is run on ion saturation mode.

On the other hand, the probe body is geometrically modelled by introducing a solid obstacle with sheath boundary condition in the middle of the plasma. The probe covers an area of  $32 \rho_L$  in the poloidal direction and occupies radially the second half of the computationnal zone. In the parallel direction the probe is infinitely thin, which seems reasonable when considering the size of the probe in comparison to the parallel length  $L_{||}$  of the plasma. At least, the probe body is taken conductive, but could just as well be chosen insulating, as we will mostly focus on density and flux perturbations.

## 3 Polarisation of the divertor probe

As stated in previous works [18,20,21], the Langmuir probe in ion saturation mode impacts the surrounding plasma and could give measurements leading to an underestimation of the plasma quantities. An illustration of the perturbation is given in Fig. 2 : the parallel current drawn by the probe is maximum at the front of the probe, decreasing along and spreading across the magnetic field lines. Following the Ohms law Eq. (3), this current has to come from a parallel gradient of potential and thus requires that the plasma in front of the probe stays at a different potential than the one of the unperturbed plasma. The perpendicular electric field which rises then gives birth to an ExB vortex around all the flux tube, preventing the turbulent plasma to reach the probe tip. To

<sup>1</sup> with a typical SOL electronic temperature  $T_0 \approx 100$  eV,  $V_p = -3$  corresponds to approximately -300V

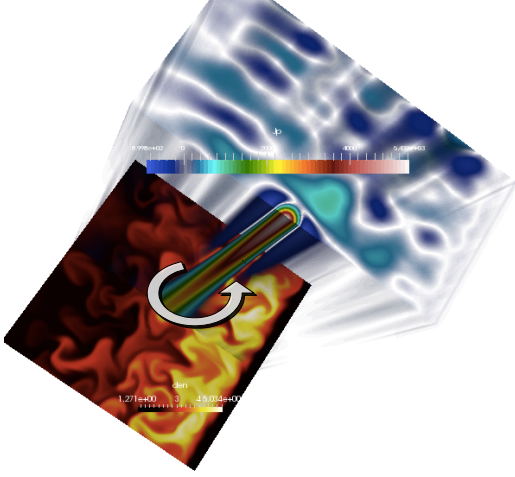


**Fig. 2** 3D view of  $J_{\parallel}$  from the top, where the probe is located. The white/transparent color indicates zero current. The bottom plan shows the XY density map in strong SOL electrostatic turbulence.

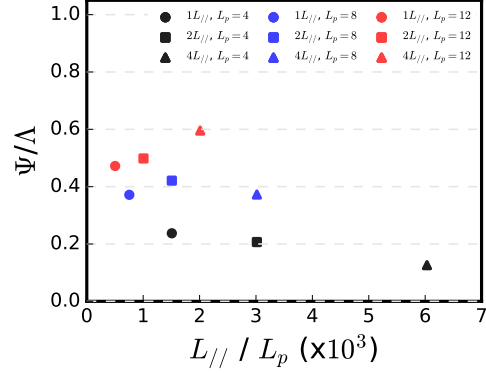


**Fig. 3** Amplitude of the perturbation in front of the probe versus the ratio of the parallel to the probe lengths. Circles are for parallel length of  $6 \times 10^3$ , squares and triangles are respectively for twice and fourth times the first  $L_{\parallel}$ . Colors show probes of the same sizes.

study this phenomenon, we define  $\Psi = \Lambda - \Phi_p$ , the difference of potential between the front of the probe and the unperturbed plasma, which characterizes the magnitude of the perturbation and thus the strength of the vortex. We also look at  $l_{\parallel}$ , the parallel extension of the perturbation.

In a semi-infinite plasma, the perturbation would extend along the field lines until the current transported across the magnetic field compensates the current drawn by the probe  $J_{\parallel p} = l_{\parallel} \nabla_{\perp} \cdot \mathbf{J}_{\perp}$ . Considering the turbulent perpendicular transport of current around the probe as an hyper-diffusif process  $\mathbf{J}_{\perp} = -\nu_{\text{turb}} \nabla \nabla^2 \Phi$  of perpendicular scale  $L_p$ , and combining this with Eq. (3), the parallel scale  $l_{\parallel}$  of the perturbation can be estimated as :

$$l_{\parallel} = \sqrt{\frac{\eta^{-1}}{\nu_{\text{turb}}}} L_p^2 \quad (5)$$

Then, the integration of the current divergence equation along the parallel direction from the probe to  $l_{\parallel}$  where the perturbation vanish and no parallel current exists let us express the amplitude of the perturbation as :

$$\Psi \approx \sqrt{\frac{\eta}{\nu_{\text{turb}}}} L_p^2 = l_{\parallel} \eta \quad (6)$$

Fig. 3 shows the amplitude of the perturbation normalized to the floating potential as a function of the ratio  $L_{\parallel}/L_p$ . There is two immediate observations : the first one is that  $\Psi$  does depend on the parallel length of the domain  $L_{\parallel}$ , in contradiction with the simple semi-infinite plasma assumption, where the perturbation should vanish at  $l_{\parallel} \ll L_{\parallel}$ . The second observation, which accords well to Eq. (6), is that at a fixed  $L_{\parallel}$ , a larger probe will produce a larger perturbation.

On another hand, we could have expected that increasing the parallel length would lead to weaken the perturbation as the perpendicular current would have been collected on a longer area. This is correct for the small probe  $L_p=4$ , but in contradiction with the results of the simulations for probes of size  $L_p=8$  and  $L_p=12$ . This difference can however be explained when reconsidering the semi-infinite plasma hypothesis : as a matter of a fact, the SOL plasma takes its place between the two sides of the limiter/divertor separated in our simulations by a parallel length of  $6 \times 10^3 - 2 \times 10^4$  (hence around 5m-20m, in a small tokamak with  $T_e^{(\text{SOL})} \approx 100\text{eV}$ ). With a parallel resistivity  $\eta$  of  $10^{-5}$ , the parallel scale of the perturbation is of the same order or even exceed the parallel length of the system :  $l_{\parallel}/L_{\parallel} \in [1,10]$ . The perturbation reaches thus easily the opposite wall, drawing current directly from it. In this case, the probe IV characteristics should be interpreted as those of double probes.

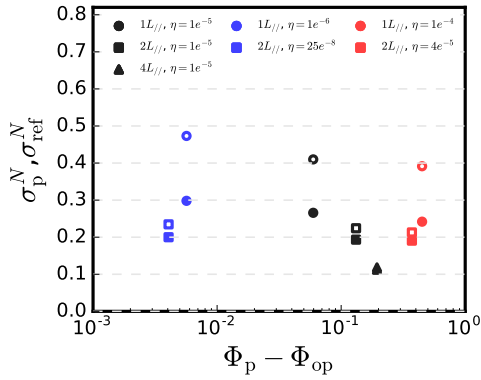


**Fig. 4** Standard deviations of density fluctuations in front of the probe (filled symbols) in comparison with the reference case (empty symbols) as a function of the potential difference between the walls. In blue on the left (small electric field), are the "conductive" cases with a low  $\eta$ . On the right (high electric field) are the "resistive" cases. Circles, squares and triangle are respectively for the base parallel length, times two and four.

Supposing now that the total perpendicular current divergence is low enough (with a very short parallel length for example) to consider  $\nabla_{\parallel} \cdot \mathbf{j} = 0$  giving a parallel current constant all along the field line and equal to the saturation current drawn by the probe. Inserting in Eq. (3) then gives :

$$j_{\parallel} = -\eta^{-1} \nabla_{\parallel} \Phi = j_{\text{sat}} \quad \text{and thus} \quad \Phi_{\text{opp}} - \Phi_p = L_{\parallel} \eta j_{\text{sat}} \quad (7)$$

Moreover, as no current comes from the perpendicular direction, the current drawn by the probe has to come entirely from the opposite wall. Expressing  $\Phi_{\text{opp}}$  with the sheath theory and substituting the saturation currents, we can see that when the perpendicular current divergence is weak :

$$\Phi_p = \Lambda - \ln \left( 1 + \frac{N_p}{N_{\text{opp}}} \right) - L_{\parallel} \eta N_p \quad (8)$$

In this situation, the perturbation in front of the probe grows when  $L_{\parallel}$  increases. For a given probe size, two behaviours are then in competition depending on the total divergence of the perpendicular current, and there is a maximum of the amplitude of the perturbation at a specific  $L_{\parallel}$ , which can be seen on Fig. 3 for the  $L_p=8$  probe size.

Another way to look at  $\Psi$  is considering it as an adaptation to the probe voltage : indeed, rewriting the definition of  $\Psi$  as  $\Phi_p = \Lambda - \Psi = \Lambda - \alpha V_p$  let us define  $\alpha = \Psi/V_p$ , an accommodation factor of the plasma potential to the probe voltage, positive and even between zero and one. Then in sweeping operations to measure IV characteristics, if the plasma potential adapts to the probe voltage, the electron current drawn by the probe should also be affected :

$$J_{\parallel p}^e = N_p \exp(\Lambda - \Phi_p + V_p) = N_p \exp(V_p(1 - \alpha)) \quad (9)$$

As a consequence, we see that if  $\alpha$  differs significantly from zero, the measured slope on the IV characteristic,  $T_e$ , will always be overestimated, by the factor  $(1 - \alpha)^{-1}$ .

Let us look now at the effect of  $\eta$  on the perturbation. When the probe is run in ion saturation mode, we are mostly interested by the density perturbation just in front of it. Eqs. (5), (6) and (8) tell that increasing the resistivity should lead to a stronger perturbation, with a lower parallel extension. Also, when  $l_{\parallel}$  is small enough, we can expect the transport barrier created by the vortex to act only on a part of the field line, and consequently that it exists a plasma refilling of the probe channel by parallel transport from the other side of the flux tube. On the contrary, if  $l_{\parallel}$  is long in comparison to  $L_{\parallel}$ , the perturbation should be constant along the field line, reaching the opposite wall, and the vortex would prevent the plasma to enter the probe channel from either sides. Less obvious on the mean plasma density, this effect is clear on the fluctuations levels, as showed on Fig. 4, from which we can extract two main trends :

1. Fluctuations are largely reduced in comparison to the unperturbed case, when the parallel length  $L_{\parallel}$  is small, which is less evident when increasing the resistivity.
2. Increasing the resistivity leads to a small reduction of  $\sigma_N$  and  $\sigma_{\text{ref}}$ , but the principal effect is the increase of the parallel electric field.

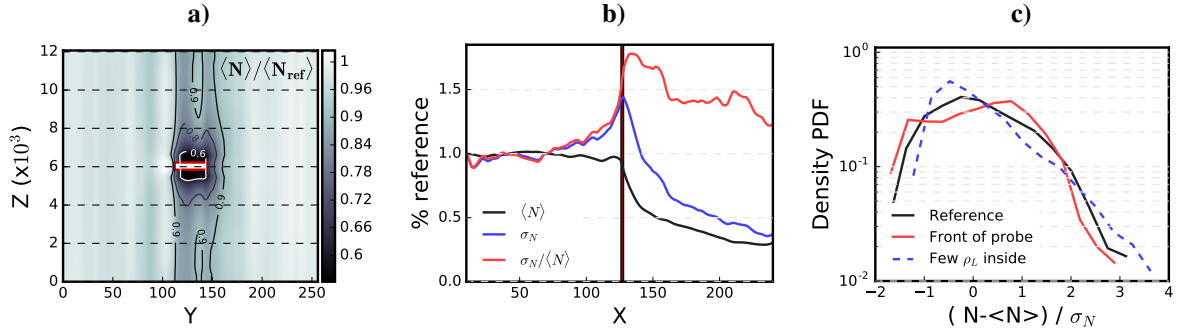


**Fig. 5** **a)** Probe shadow in the poloidal plane. Map of the mean plasma density in comparison with the unperturbed case around the probe. The probe, white, is situated at the middle of the field lines. **b)** Radial profile of the mean density, standard deviations and standard deviation normalized to  $\langle N \rangle$  to the unperturbed reference case. The black line denotes the contact point with the probe. **c)** PDFs of density for the reference case, just in front of and few Larmor radius inside the probe shadow.

In the case of ITER, where the plasma will be hot and highly conductive, we can expect a strong connection of the perturbation between the two sides of the divertor. The flushed mounted probes should then act like double probes, the current being limited by the sheath of the opposite wall.

## 4 Reciprocating probe body and synthetic Mach measurements

In this section, we study for the first time the impact of a probe body inserted in the SOL plasma with a full 3D turbulent code, at the scale of the Larmor radius. The geometry and the dimensions of the problem are sketched on Fig. 1 of the model section. After a description of the main impacts of the probe on the SOL plasma characteristics, we will reconstruct and study a synthetic Mach probe measurement following the Hutchinson theory [8].

### 4.1 Perturbation the SOL plasma due to the probe body

The first principal effect of the insertion into the SOL of a solid object is the creation of its own secondary pre-sheaths, the object's shadow [?]. Indeed, as the length of the field lines is divided by two and the loss surface for the plasma doubles, it will exist, on the both side of the probe, two areas of reduced density, where the radial decay length is strongly shortened. This effect is clearly recovered in the simulations, as we can see on the Figs. 5 : the shadow of the probe extends along all the field lines, the plasma density is depleted in the probe shadow, from 20% to more than 40%, and this just few  $\rho_L$  after the first contact between the plasma and the probe. The plasma potential, which responds to the plasma pressure accordingly to the Boltzmann relation, is also deeply impacted : the potential difference which emerges between the unperturbed plasma and the probe shadow gives birth to perpendicular electric fields, radials along the borders of the probe and poloidal in front of it. As in the flushed probe cases, this perpendicular electric field creates strong transport barriers all around the shadow, accentuating the plasma depletion.

These two effects, namely the dump of plasma density due to presence of the probe and the transport barriers, both impact the plasma fluctuations inside the probe shadow, either by "reducing" the frequency of bursts and also by increasing their relative importance in comparison to  $\langle N \rangle$ . In front of the probe, where the poloidal transport barrier emerges, the PDF shows that there is much more middle or mixed events, corresponding to avalanches stopped and redirected. More inside the probe shadow, we clearly observe a modification of the kurtosis of the PDF indicating less frequent but more important events. They correspond to the avalanches which pass through the barrier, with a density relatively much more important than the plasma in the probe shadow.

In this simple case, without parallel or poloidal mean flows, it should be

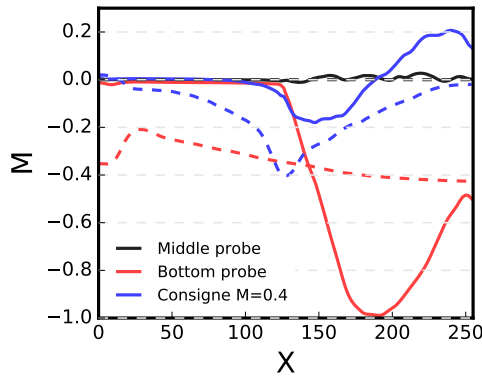


**Fig. 6** Standard deviations of density fluctuations in front of the probe (filled symbols) in comparison with the reference case (empty symbols) as a function of the potential difference between the walls. In blue on the left (small electric field), are the "conductive" cases with a low  $\eta$ . On the right (high electric field) are the "resistive" cases. Circles, squares and triangle are respectively for the base parallel length, times two and four.

## 4.2 Synthetic Mach measurements

### 4.2.1 Measurements without parallel flow

### 4.2.2 Measurements in the presence of parallel flow

## 5 Discussion

## 6 Conclusion

**Acknowledgements** This work has been financially supported by the French National Research Agency through project ANR-11-BS09-023 (SEDIBA). It has been carried out within the framework of the EUROfusion Consortium with a funding from the Euratom research and training programme 2014-2018 in the frame of project WP14-ER-01/CEA-09. The views and opinions expressed herein do not necessarily reflect those of the European Commission. This work was granted access to the HPC resources of Aix-Marseille Universit financed by the project Equip@Meso (ANR-10-EQPX-29-01) of the programme "Investissements d'Avenir" supervised by the Agence Nationale pour la Recherche. It also used HPC resources from GENCI-IDRIS in the frame of project i2015056912.

## References

- [1] I. Langmuir, *Journal of the Franklin Institute* **196**(6), 751 – 762 (1923).
- [2] I. Langmuir, *Phys. Rev.* **33**(Jun), 954–989 (1929).
- [3] L. Tonks and I. Langmuir, *Phys. Rev.* **34**(Sep), 876–922 (1929).
- [4] D. Bohm, Minimum ionic kinetic energy for a stable sheath, 1949.
- [5] F. F. Chen, J. D. Evans, and W. Zawalski, Electric probes, in: *In Plasma Diagnostic Techniques*, edited by Huddleston, RH and Leonard, SL, (1965).
- [6] G. F. Matthews, *Plasma Phys. Control. Fusion* **36**(10), 1595 (1994).
- [7] P. C. Stangeby, *The plasma boundary of magnetic fusion devices*, Plasma physics series (Taylor & Francis, New York, 2000).
- [8] I. H. Hutchinson, *Principles of Plasma Diagnostics*, second edition (Cambridge University Press, 2002), Cambridge Books Online.
- [9] P. Stangeby, *Journal of Nuclear Materials* **121**, 36 – 40 (1984).
- [10] I. H. Hutchinson, *Physics of Fluids* **30**(12), 3777–3781 (1987).
- [11] G. F. Matthews and P. C. Stangeby, *Journal of Physics D: Applied Physics* **22**(5), 644 (1989).
- [12] I. H. Hutchinson, *Phys. Fluids B* **3**(3), 847–856 (1991).
- [13] V. A. Rozhansky, A. A. Ushakov, and V. S. P., *Nucl. Fusion* **39**(5), 613 (1999).
- [14] I. H. Hutchinson, *Phys. Rev. Lett.* **101**(Jul), 035004 (2008).
- [15] P. C. Stangeby, *Plasma Physics and Controlled Fusion* **37**(9), 1031 (1995).
- [16] I. H. Hutchinson and L. Patacchini, *Plasma Physics and Controlled Fusion* **52**(12), 124005 (2010).
- [17] R. A. Pitts and P. C. Stangeby, *Plasma Physics and Controlled Fusion* **32**(13), 1237 (1990).
- [18] P. Ghendrih, Y. Sarazin, G. Attuel, S. Benkadda, P. Beyer, G. Falchetto, C. Figarella, X. Garbet, V. Grandgirard, and M. Ottaviani, *Nucl. Fusion* **43**(10), 1013 (2003).
- [19] S. J. Zweben, R. J. Maqueda, A. L. Roquemore, C. E. Bush, R. Kaita, R. J. Marsala, Y. Raiteses, R. H. Cohen, and D. D. Ryutov, *Plasma Physics and Controlled Fusion* **51**(10), 105012 (2009).



- [20] C. Colin, P. Tamain, P. Ghendrih, F. Schwander, and E. Serre, *Contrib. Plasma Phys.* **54**(4-6), 543–548 (2014).
- [21] R. Futtersack, C. Colin, P. Tamain, G. Ciraolo, P. Ghendrih, Y. Marandet, F. Schwander, and E. SERRE, First principle modeling of interplay between Langmuir probe and edge plasma turbulence, in: 15th Plasma edge theory in Fusion devices conference, (Nara, Japan, September 2015).
- [22] S. J. Zweben, J. A. Boedo, O. Grulke, C. Hidalgo, B. LaBombard, R. J. Maqueda, P. Scarin, and J. L. Terry, *Plasma Phys. Control. Fusion* **49**(7), S1 (2007).
- [23] P. Tamain, H. Bufferand, G. Ciraolo, C. Colin, D. Galassi, P. Ghendrih, F. Schwander, and E. Serre, *Journal of Computational Physics* pp. – (2016).
- [24] P. Tamain, P. Ghendrih, H. Bufferand, G. Ciraolo, C. Colin, N. Fedorczak, N. Nace, F. Schwander, and E. Serre, *Plasma Phys. Control. Fusion* **57**(5), 054014 (2015).